Electronic transport in carbon nanotubes using the transfer-matrix method

Umegaki, Toshihito
Ogawa, Matsuto
Makino, Yasuyuki
Miyoshi, Tanroku

(Citation)
Journal of Applied Physics,96(11):6669-6678

(Issue Date)
2004-12-01

(Resource Type)
journal article

(Version)
Version of Record

(URL)
https://hdl.handle.net/20.500.14094/90000824

Electronic transport in carbon nanotubes using the transfer-matrix method

Toshihito Umegaki,[a] Matsuto Ogawa, Yasuyuki Makino, and Tanroku Miyoshi
Graduate School of Science and Technology, Kobe University, 1-1 Rokkodai-cho, Nada-ku, Kobe City, 657-8501, Japan

(Received 15 March 2004; accepted 23 August 2004)

We have studied the basic conductive characteristics in carbon nanotubes (CNTs) for the purpose of application to a high-frequency device. In the analysis, the current flow in the CNTs is viewed as the quantum transport of electronic waves. First, we analyzed the dispersion relations of electronic waves in the CNTs based on the linear combination of atomic orbitals expansion method. In addition, we investigated the current-density distributions around the circumference of the CNTs and the current-voltage characteristics by using the transfer-matrix method. As a result, the current distributions were found to be significantly controlled by both the chirality of the CNTs and the position of the current sources around the circumference. Based on these results, we propose herein a ferrite device that acts as a filter in the terahertz frequency domain. In this device, the high-frequency current flowing on the CNTs may excite and receive directly the spin waves in the ferrite film beneath them, and the operating wavelength may be controlled by means of the chirality via the current-density distributions on the CNTs. In addition, we found that the performance of the device can be improved by using the *p*-type CNTs as the excitation electrodes rather than the intrinsic CNTs. © *2004 American Institute of Physics*. [DOI: 10.1063/1.1806550]

I. INTRODUCTION

Since the discovery of carbon nanotubes (CNTs),[1] the properties of CNTs have attracted a great deal of interest due to their unique structures and promising properties. For example, CNTs have an ample mechanical strength and a higher conductivity than the conventional materials such as iron and silicon. It has been quite difficult to fabricate electrodes of less than 100 nm in conventional semiconductor devices such as integrated circuits. However, the diameters of CNTs can be easily controlled at sizes as small as several nanometers. In addition, the great advantage of CNTs over the conventional materials is that a diameter control can be achieved by means of self-organization and ballistic conductivities. One of the main considerations in applying such CNTs to electronic devices, however, is controlling the conductivity and the current-density distributions on the CNTs by means of their chirality.

In this paper, we study the basic conductive characteristics in CNTs to apply to a high-frequency device. The current in the CNTs is rigorously treated within the framework of quantum mechanics. In the next section, the models of CNTs are described and the band structures of CNTs are analyzed based on the linear combination of atomic orbitals (LCAO) expansion method. In particular, the difference in the band structures of the CNTs depending on the chirality is discussed. In Sec. III, the calculation method for the analysis of the electron-transport properties in the CNTs by the transfer-matrix (TM) method is presented. The results of the calculated *I-V* characteristics are also discussed in this section. In Sec. IV based on the obtained results, we propose a ferrite device that will work as a bandpass filter in the terahertz frequency domain. The relationships between the performance of the device and the position of the Fermi level in the CNTs are discussed. Such devices may cultivate a field of application for the CNTs. And in the final section, the conclusions are summarized.

II. BAND STRUCTURES OF CNTS WITH ARBITRARY CHIRALITY

Figure 1 shows a schematic model of a CNT under an applied bias voltage V_0. The left and right graphite unit cells (GUCs) in Fig. 1 correspond to the *zigzag* and *armchair* CNTs, respectively. The graphite sheet consists of GUCs, as shown in the lowest figure, where "▲" or "▼" stands for a carbon atom on the *A* site or *B* site, respectively, in the honeycomb lattice. Since the CNT is comprised of coaxially

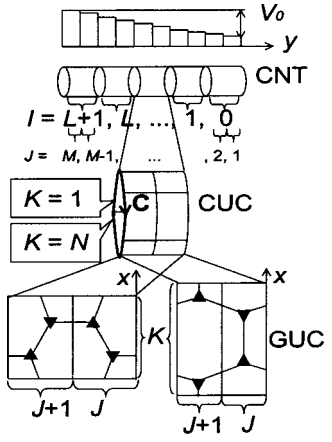

FIG. 1. Schematic models of CNTs viewed as the coaxially rolled graphite sheets under a biased condition: the left and right GUCs correspond to the *zigzag* and *armchair* CNTs, respectively.

[a]Present address: Graduate School of Science and Technology, Kobe University, 1-1 Rokkodai, Nada-ward, Kobe City, 657-8501, Japan; electronic mail: 993d914n@y01.kobe-u.ac.jp

rolled two-dimensional (2D) graphite sheet, each CNT unit cell (CUC) consists of GUCs and the entire CNT is comprised of CUCs, as shown in the middle figure. The circumferential vector of the tube **C** is called the chiral vector and is generally expressed as $\mathbf{C}=n_1\mathbf{a}+n_2\mathbf{b}$, where **a** and **b** are the primitive translational vectors in the honeycomb lattice. Usually, a CNT with this chiral vector is called an (n_1,n_2) or a *chiral* nanotube. In particular, an $(n,0)$ nanotube is called a *zigzag* nanotube and an (n,n) nanotube is called an *armchair* nanotube. The uppermost figures show the potential distribution under a biased condition. The potential in each CUC is assumed to be constant, for simplicity.

To calculate the band structures of the CNTs without an applied bias voltage, we adopt a simple tight-binding model in which an on-site energy ϵ_0 on a carbon atom and a hopping-energy γ between the nearest neighbors are assumed. We use the following values throughout this paper: $\epsilon_0=-2.18$ eV and $\gamma=2.31$ eV.[2]

The Bloch functions at sites *A* and *B* can be expressed in terms of a linear combination of atomic orbitals as

$$\phi_{\mathrm{A}\mathbf{k}}(\mathbf{r}) = \sqrt{\frac{L+2}{NM}}\sum_{\mathbf{r}_\mathrm{A}}^{\mathrm{CUC}} e^{i\mathbf{k}\cdot\mathbf{r}_\mathrm{A}}\Phi(\mathbf{r}-\mathbf{r}_\mathrm{A}),$$
$$\phi_{\mathrm{B}\mathbf{k}}(\mathbf{r}) = \sqrt{\frac{L+2}{NM}}\sum_{\mathbf{r}_\mathrm{B}}^{\mathrm{CUC}} e^{i\mathbf{k}\cdot\mathbf{r}_\mathrm{B}}\Phi(\mathbf{r}-\mathbf{r}_\mathrm{B}), \tag{1}$$

where **k** is the wave vector, Φ is the π atomic orbital of a carbon atom, *N* is the number of GUCs around the circumference of the CUC, which is equal to *n* for the *zigzag* types and *armchair* nanotubes, *M* is the number of GUCs along the CNT, *L* is the number of CUCs along the CNT, and $\mathbf{r}_\mathrm{A}$ and $\mathbf{r}_\mathrm{B}$ are the positions of the sites *A* and *B*, respectively. The wave-function $\Psi_\mathbf{k}(\mathbf{r})$ can be expanded by a linear combination of the Bloch functions $\phi_{\mathrm{A}\mathbf{k}}(\mathbf{r})$ and $\phi_{\mathrm{B}\mathbf{k}}(\mathbf{r})$, that is

$$\Psi_\mathbf{k}(\mathbf{r}) = \mathrm{C}_A\phi_{\mathrm{A}\mathbf{k}}(\mathbf{r}) + \mathrm{C}_B\phi_{\mathrm{B}\mathbf{k}}(\mathbf{r}). \tag{2}$$

Substituting Eq. (2) into the Schrödinger equation, we can easily obtain the *E*-**k** dispersion relations of the graphite sheet as

$$E(\mathbf{k}) = \epsilon_0 \pm \gamma \times\sqrt{1+4\cos^2\left(\frac{k_x a}{2}\right)+4\cos\left(\frac{k_x a}{2}\right)\cos\left(\frac{\sqrt{3}k_y a}{2}\right)}, \tag{3}$$

where *a* is the lattice constant and the minus sign $(-)$ and plus sign $(+)$ denote the bonding and antibonding energy bands, respectively. The obtained results exactly coincide with the dispersion relation of the graphite sheet.[2] Figure 2 shows the equipotential contour plot of the dispersion relation in the graphite sheet. The + branch and − branch energies become degenerated $(=\epsilon_0)$ at point K, $\epsilon_0\pm\gamma$ along the line MM, and $\epsilon_0\pm3\gamma$ at point Γ,[3] respectively. As stated before, because a CNT consists of a coaxially rolled 2D graphite sheet, CNT dispersion curves can be obtained by slicing the contour along an appropriate line determined by its chiral vector. Analytically, the dispersion relation of a CNT with the (n,m) chirality can be obtained by imposing the periodic boundary conditions in the circumferential direction,

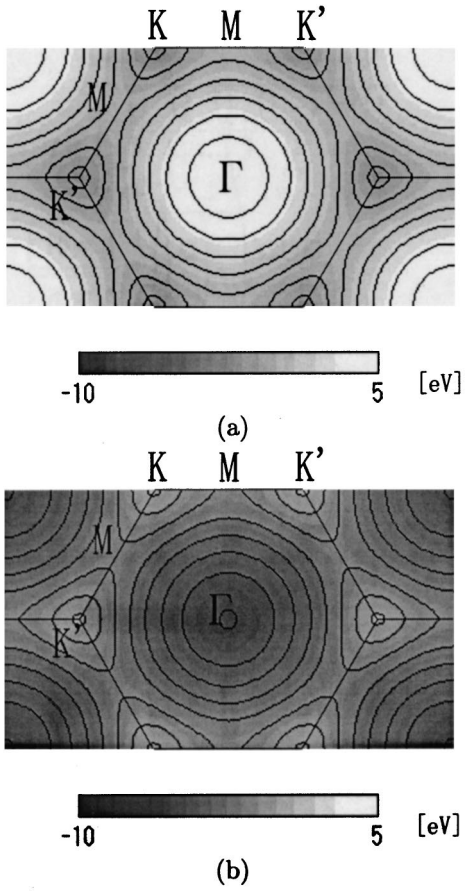

FIG. 2. Equipotential plot of the energy bands in a graphite sheet: (a) antibonding energy band (+ branch) and (b) bonding energy band (− branch).

$$\Psi_\mathbf{k}(\mathbf{r}+\mathbf{C}) = \Psi_\mathbf{k}(\mathbf{r})\exp(i\mathbf{k}\cdot\mathbf{C}) = \Psi_\mathbf{k}(\mathbf{r}). \tag{4}$$

From this boundary condition, we obtain the *quantized* wave vectors in the *x* direction as

$$k^x = \frac{2\pi i^x}{\sqrt{n^2+nm+m^2}a},\ (i^x = 0,\pm1,\pm2,\cdots). \tag{5}$$

From Eqs. (3) and (5), we obtain the eigenvalue equation of the *chiral* nanotube as

$$(\epsilon_0-E)^2-\gamma^2[1+8\cos(k^x x_1+k^y y_1) \times\cos(k^x x_2+k^y y_2)\cos(k^x x_3+k^y y_3)]=0, \tag{6}$$

where

$$x_1=\frac{(n-m)a}{4\sqrt{n^2+nm+m^2}},\quad y_1=\frac{-\sqrt{3}(n+m)a}{4\sqrt{n^2+nm+m^2}},$$
$$x_2=\frac{(2n+m)a}{4\sqrt{n^2+nm+m^2}},\quad y_2=\frac{-\sqrt{3}ma}{4\sqrt{n^2+nm+m^2}}, \tag{7}$$
$$x_3=\frac{(n+2m)a}{4\sqrt{n^2+nm+m^2}},\quad y_3=\frac{\sqrt{3}na}{4\sqrt{n^2+nm+m^2}}.$$

We can evaluate the dispersion curves of the CNT with the arbitrary chirality from Eq. (6). For the clarity of understanding, however, we confine ourselves to the analysis of

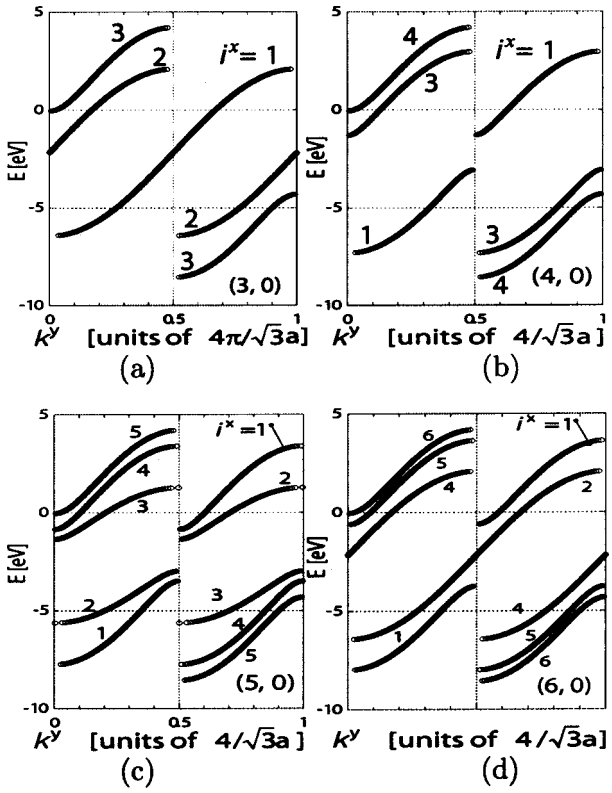

FIG. 3. Dispersion curves of the *zigzag* CNTs: chirality=$(n,0)$; n=(a) 3, (b) 4, (c) 5, and (d) 6, respectively.

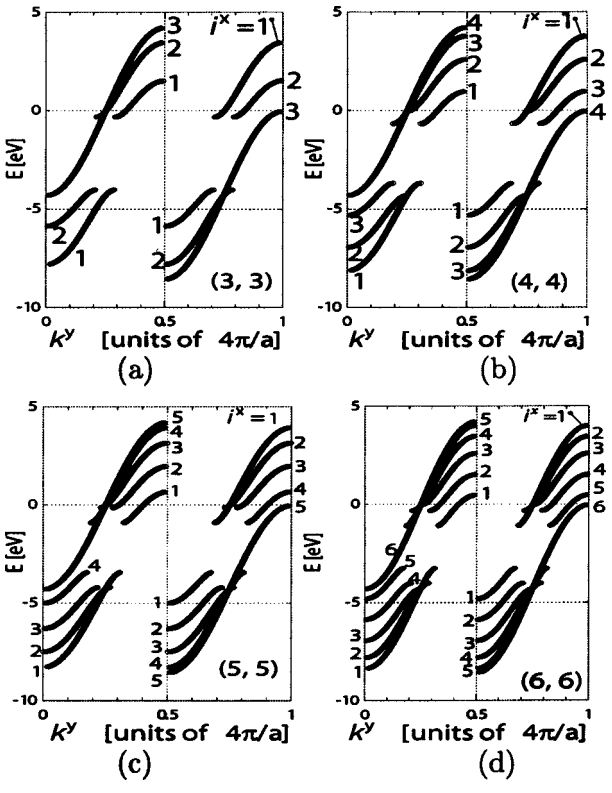

FIG. 4. Dispersion curves of the *armchair* CNTs: chirality=(n,n); n =(a) 3, (b) 4, (c) 5, and (d) 6, respectively.

the *zigzag* and *armchair* CNTs in this paper.

The dispersion relation of the *zigzag* CNTs can be obtained by simply setting $m=0$ in Eqs. (5) and (6). Figure 3 shows the band structures of the *zigzag* CNTs with $n=(a)3$, (b)4, (c)5, and (d)6, respectively. We have plotted only the branches with the positive group velocities. This is because it is convenient to classify the branches according to the positive or negative group velocity when calculating the electronic current propagating in the CNTs. The branches having the negative group velocities can be obtained by simply taking the mirror reflection of the positive branches at the center of the Brillouin zone due to the symmetric properties of the graphite sheet band structure. It should be noted that the dispersion curves always cross for the case $n=3N$, with N being an integer. In other words, the energy gap disappears and the *zigzag* tubes become metallic. Among the four CNTs shown in Fig. 3, the (3, 0) and (6, 0) CNTs are metallic.

On the other hand, the dispersion relations of the *armchair* CNTs are obtained by setting $m=n$ in Eqs. (5) and (6). Figure 4 shows the band structures of the *armchair* CNTs. Again, the energy gap always vanishes for the *armchair* CNTs, i.e., they are always metallic. Due to the graphite sheet band structure, the i^x given in Eq. (6) is restricted within $-(n-1), -(n-2), \ldots, 0, 1, 2, \ldots, n$ for both the *zigzag* and *armchair* CNTs. We plotted only the branches with $i^x = 1, 2, \ldots, n$, because it is convenient to classify the branches according to the circumferential direction when we calculate the electronic current propagating in the CNTs.

III. CURRENT IN CNTS

In this section, a quantum-mechanical method is described for the calculation of the current in CNTs. We use the TM method[4] to analyze the propagation of electron waves in the CNTs. The TM method will be described in detail, because we are interested in not only the quantum conductance but also in the current distribution in the CNTs for a practical application, as will be described in Sec. IV.

A. Boundary conditions at the interface of CUCs

As shown in Fig. 1, when an external bias V_0 is applied to the CNT, there is a potential difference between the neighboring two CUCs, because we have assumed the potential to be constant in each CUC for a simplicity. For a more precise determination of the voltage drop in the CNT, the potential should be determined by the Poisson equation.[5] In order to conserve the probability density flow as well as the probability density, the existing electron waves must be connected appropriately at the interface of the neighboring CUCs, i.e., between J and $J+1$. Let $\mathbf{F}_J$ be the amplitude vector comprised of a set of amplitudes expressed in terms of the Bloch functions in the Jth CUC. Then, the average probability current flow $\overline{J_J}$ is expressed as follows using the Hellmann-Feynman theorem[6] (see Appendix):

$$\overline{J_J} = \left[\frac{1}{\hbar} \frac{\partial E}{\partial k^y} \right]_J |\mathbf{F}_J|^2. \tag{8}$$

To conserve the average probability current flow and probability density, we impose boundary conditions equivalent to those in the effective-mass theory[7,8]

$$\begin{cases} \mathbf{F}_J & \text{is continuous at the interface,} \\ \dfrac{1}{\hbar}\dfrac{\partial \mathrm{E}}{\partial \mathrm{k}^y}\mathbf{F}_J & \text{is continuous at the interface.} \end{cases} \tag{9}$$

B. Transfer matrices of CNTs

The amplitude in the Kth GUC is expressed as

$$\begin{aligned} F_{J,K}(x,y) = &\{A_{J,K}\exp[ik^x(x-x_{J,K}^C)] \\ &+ C_{J,K}\exp[-ik^x(x-x_{J,K}^C)]\}\exp[ik_J^y(y-y_{J,K}^C)] \\ &+ \{B_{J,K}\exp[ik^x(x-x_{J,K}^C)] + D_{J,K} \\ &\times\exp[-ik^x(x-x_{J,K}^C)]\}\exp[-ik_J^y(y-y_{J,K}^C)], \end{aligned} \tag{10}$$

where the coordinates x and y run within the GUC. The amplitude $F_{J,K}(x,y)$ can be expressed in terms of the propagating waves toward the right (+) and the left (−) as

$$\begin{aligned} F_{J,K}^{y+}(x,y) = &\{A_{J,K}\exp[ik^x(x-x_{J,K}^C)] + C_{J,K} \\ &\times\exp[-ik^x(x-x_{J,K}^C)]\}\exp[ik_J^y(y-y_{J,K}^C)], \end{aligned} \tag{11a}$$

$$\begin{aligned} F_{J,K}^{y-}(x,y) = &\{B_{J,K}\exp[ik^x(x-x_{J,K}^C)] + D_{J,K} \\ &\times\exp[-ik^x(x-x_{J,K}^C)]\}\exp[-ik_J^y(y-y_{J,K}^C)]. \end{aligned} \tag{11b}$$

Applying the continuity conditions in Eq. (9), we obtain the following conditions at the interface $y=(y_{J,K}^C+y_{J+1,K}^C)/2$:

$$F_{J+1,K}^{y+} + F_{J+1,K}^{y-} = F_{J,K}^{y+} + F_{J,K}^{y-}, \tag{12a}$$

$$\frac{\partial E}{\partial k_{J+1}^y}F_{J+1,K}^{y+} - \frac{\partial E}{\partial k_{J+1}^y}F_{J+1,K}^{y-} = \frac{\partial E}{\partial k_J^y}F_{J,K}^{y+} - \frac{\partial E}{\partial k_J^y}F_{J,K}^{y-}. \tag{12b}$$

Equations (12a) and (12b) are expressed in a matrix equation using the transfer-matrix M_J as

$$\begin{pmatrix} A_{J+1,K}+C_{J+1,K} \\ B_{J+1,K}+D_{J+1,K} \end{pmatrix} = M_J \begin{pmatrix} A_{J,K}+C_{J,K} \\ B_{J,K}+D_{J,K} \end{pmatrix}, \tag{13a}$$

where

$$M_J = \begin{pmatrix} \alpha_+^{(J)}P^{(J)} & \alpha_-^{(J)}Q^{(J)} \\ \alpha_-^{(J)}/Q^{(J)} & \alpha_+^{(J)}/P^{(J)} \end{pmatrix}. \tag{13b}$$

The matrix elements of the transfer matrix are

$$\alpha_\pm^{(J)} = \frac{1}{2}\left(1 \pm \frac{\partial E/\partial k_J^y}{\partial E/\partial k_{J+1}^y}\right), \tag{14a}$$

$$P^{(J)} = \exp\left[i(k_{J+1}^y + k_J^y)\frac{y_{J+1}^C - y_J^C}{2}\right], \tag{14b}$$

$$Q^{(J)} = \exp\left[i(k_{J+1}^y - k_J^y)\frac{y_{J+1}^C - y_J^C}{2}\right]. \tag{14c}$$

The entire transfer-matrix M^{tot} is obtained from Eq. (13b) by multiplying each transfer-matrix M_J from $J=1$ to $M-1$ as

$$M^{\mathrm{tot}} = M_{M-1}\cdots M_J\cdots M_1. \tag{15}$$

Note that we have labeled the indices from M (input) to 1 (output) in Eq. (15). The transmission coefficient $\mathcal{D}_{(M,K')\to(1,K)}$ is defined as the ratio of the input and output probability currents, which are obtained from the (1, 1) element of the matrix M^{tot} as

$$\begin{aligned} \mathcal{D}_{(M,K')\to(1,K)} &= \frac{\partial E/\partial k_1^y |A_{1,K}+C_{1,K}|^2}{\partial E/\partial k_M^y |A_{M,K'}+C_{M,K'}|^2} \\ &= \frac{1}{|M^{\mathrm{tot}}{}_{1,1}|^2}\frac{\partial E/\partial k_1^y |A_{1,K}+C_{1,K}|^2}{\partial E/\partial k_M^y |A_{1,K'}+C_{1,K'}|^2}. \end{aligned} \tag{16}$$

Similarly, applying the boundary conditions to the x direction, we can obtain the transmission coefficient as

$$\mathcal{D}_{(M,K')\to(1,K)} = \cos^2[k^x(x_{K'}^C - x_K^C)]\frac{1}{|M^{\mathrm{tot}}{}_{1,1}|^2}\frac{\partial E/\partial k_1^y}{\partial E/\partial k_M^y}. \tag{17}$$

The current density $\mathcal{J}_{(M,K')\to(1,K)}$ is expressed as

$$\mathcal{J}_{(M,K')\to(1,K)} = n_c q v^y, \tag{18}$$

where n_c is the carrier concentration, q is the electronic charge (absolute value), and v^y is the group velocity. Performing a simple calculation, we finally obtain

$$\begin{aligned} \mathcal{J}_{(M,K')\to(1,K)} = &\frac{2q}{nx_{\mathrm{G}}h}\sum_{i^x,i^y}\int [f_M(E) - f_1(E)] \\ &\times \mathcal{D}_{(M,K')\to(1,K)}dE, \end{aligned} \tag{19}$$

where x_{G} is a and $\sqrt{3}a$ is for the *zigzag* and *armchair* types, respectively, and f_M and f_1 are the Fermi-Dirac distribution functions at the left and right electrodes, respectively, defined by

$$f_M(E) - f_1(E) = \frac{1}{2}\left[\tanh\left(\frac{E-E^1}{2k_BT}\right) - \tanh\left(\frac{E-E^M}{2k_BT}\right)\right], \tag{20}$$

where the Fermi level is assumed to be zero and

$$E^1 = \epsilon_0 \text{ and } E^M = \epsilon_0 + V_0. \tag{21}$$

The effect of the position of the Fermi level will be discussed later.

Since the properties of the contacts between the CNT and the metal electrodes attached to it have not been clarified either experimentally or theoretically, we consider the three specific cases of the excitation position of the electronic waves at the input terminal $J=M$ in the following:

(1) the electronic waves are excited around the entire circumference of the CNT,
(2) the electronic waves are injected into the unit cell $K'=1$ of the CNT, and
(3) the electronic waves are excited uniformly around the entire circumference of the CNT and are received as an average at each unit cell of the CNT.

In case 1, the current density $\mathcal{J}_K$ is

$$\mathcal{J}_K = \sum_{K'=1}^{n} \mathcal{J}_{(M,K')\to(1,K)} \tag{22}$$

and the total current $\mathcal{I}$ flowing from left to right is calculated, integrating $\mathcal{J}_K$ around the CNT as

$$\mathcal{I} = \frac{2q}{nh} \sum_{K,K'=1}^{n} \sum_{i_x,i_y} \int [f_M(E) - f_1(E)] \mathcal{D}_{(M,K')\to(1,K)} dE,$$

(*zigzag or armchair*). (23)

In case 2, since the summation over K' should be done only for $K'=1$, the current density $\mathcal{J}_K$ is given by

$$\mathcal{J}_K = \mathcal{J}_{(M,1)\to(1,K)} \tag{24}$$

and the total current $\mathcal{I}$ is calculated integrating $\mathcal{J}_K$ around the CNT as

$$\mathcal{I} = \frac{2q}{nh} \sum_{K=1}^{n} \sum_{i_x,i_y} \int [f_M(E) - f_1(E)] \mathcal{D}_{(M,1)\to(1,K)} dE, \tag{25}$$

(*zigzag or armchair*).

In case 3, rather than using Eq. (16), the transmission coefficient $\mathcal{D}_K$ is defined as the ratio of the input and output probability currents as

$$\mathcal{D}_K = \frac{\sum_{K'''=1}^{n} \overline{J^y}_{1,K,K'''}}{\frac{1}{N}\sum_{K',K''=1}^{n} \overline{J^y}_{M,K',K''}}, \tag{26a}$$

$$\overline{J^y}_{1,K,K'} = \frac{\partial E}{\partial k^y_{1,K}} |A_{1,K} + C_{1,K}|^2, \tag{26b}$$

$$\overline{J^y}_{M,K,K'} = \frac{\partial E}{\partial k^y_{M,K}} |M^{\mathrm{tot}}_{K\ 1,1}(A_{M,K} + C_{M,K})|^2. \tag{26c}$$

In Eq. (26), the input probability current is averaged over the input CUC, where K' runs from 1 to n. The input and output probability currents flow by the electronic waves excited at each input GUC and summed over the (M,K'')-th and (M,K''')-th GUCs, where K'' and K''' run from 1 to n. We then obtain $\mathcal{D}_K$ from the (1,1) element of the matrix M^{tot}_K. Similarly, applying the boundary conditions to the x direction (see Appendix II), we obtain the transmission coefficient as

$$\mathcal{D}_K = \frac{\sum_{K'''=1}^{n} \partial E/\partial k^y_{1,K} |2c(K,K''',k^x)|^2}{\frac{1}{n}\sum_{K',K''=1}^{n} \partial E/\partial k^y_{M,K'} |M^{\mathrm{tot}}_{K'1,1}|^2 |2c(K',K'',k^x)|^2} \tag{27a}$$

$$c(K,K',k^x) \equiv \cos[(K-K')k^x x_G]. \tag{27b}$$

The current density $\mathcal{J}_K$ is expressed as

$$\mathcal{J}_K = \int_{r_{CNT}}^{r_{CNT}+\delta z} n_c q v^y \, dz, \tag{28}$$

where n_c is the carrier concentration, q is the electronic charge (absolute value), v^y is the group velocity, r_{CNT} is the radius of the CNT, and δz is the thickness of the graphite. Performing a simple calculation (see Appendix III), we finally obtain

$$\mathcal{J}_K = \frac{2q}{nx_G h} \sum_{i^x,i^y} \int_{-\infty}^{\infty} [f_M(E) - f_1(E)] \mathcal{D}_K dE, \tag{29}$$

(*zigzag* or *armchair*).

The total current $\mathcal{I}$ flowing from left to right is calculated, integrating $\mathcal{J}_K$ around the CNT as

$$\mathcal{I} = \int_0^{nx_{GUC}} \mathcal{J}_K dx = x_{GUC} \sum_{K=1}^{n} \mathcal{J}_K, \tag{30}$$

(*zigzag* or *armchair*).

where x_{GUC} is the circumferential dimension of the GUC. Substituting Eqs. (27) and (29) into Eq. (30), we obtain

$$\mathcal{I} \frac{2q}{h} \sum_{i^x}^{1st-BZ} \int_{-\infty}^{\infty} \{f_M(E) - f_1(E)\} \times \frac{\sum_{K,K'''=1}^{n} \partial E/\partial k^y_{1,K} c^2(K,K''',k^x)}{\sum_{K',K''=1}^{n} \partial E/\partial k^y_{M,K'} |M^{\mathrm{tot}}_{K'1,1}|^2 c^2(K',K'',k^x)} dE. \tag{31}$$

C. Current density around the CNTs and *I–V* characteristics

It is important to analyze not only the $I-V$ characteristics but also the current-density distributions around the circumference of the *zigzag* CNTs in order to apply them to electronic devices. Figure 5 shows the current-density distributions around the CNTs for the bias $V_0=10$ mV. Figures 5(a)–5(d) show the results for $n=3$, 4, 5, and 6, respectively. The points indicated by the symbols ●, □, and ▲ are those for cases 1, 2, and 3, respectively. In cases 1 and 3, the current-density distribution around the circumference of the CNTs is uniform for any metallic chirality. In contrast, in case 2, the current-density distribution is nonuniform in the *zigzag* CNTs because the dispersion curve in Fig. 3 is metallic only when $i^x=n/3$ or $2n/3$, where $n=3,6,9,\ldots$.

On the other hand, Fig. 6 shows the current-density distributions around the *armchair* CNTs for the same bias. Figures 6(a)–6(d) also show the results for $n=3$, 4, 5, and 6, respectively. In contrast to Fig. 5, the distributions around the circumference are always uniform in the *armchair* CNTs because the dispersion curve in Fig. 4 is always metallic, and the argument of cos in Eq. (17) becomes $2\pi(K-K')$, when $i^x=n$. It should be emphasized that the current distributions around the CNTs are found to be controlled by both the chirality and the position of the excitation position of the electronic waves. Figures 7 and 8 show the $I-V$ characteristics of the CNTs of the *zigzag* and *armchair* types, respec-

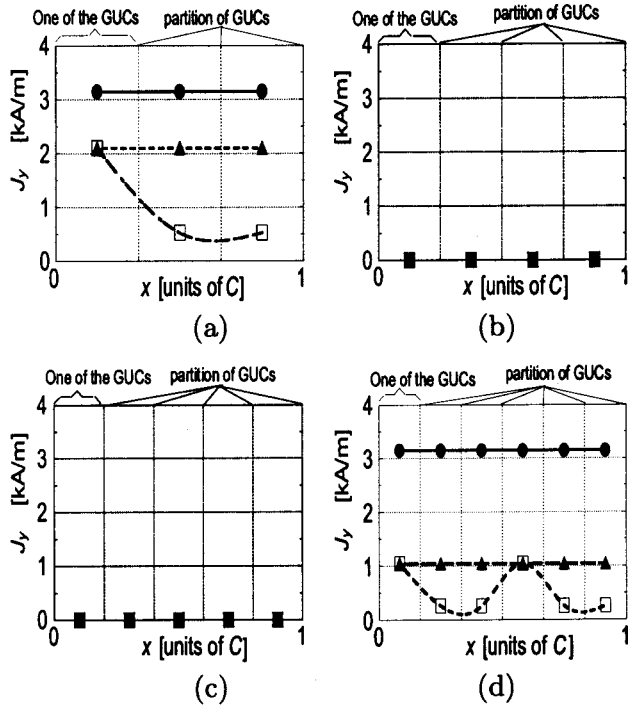

FIG. 5. Current-density distributions around the CNTs at the *zigzag* CNTs: $L=20$; $n=$(a) 3, (b) 4, (c) 5, and (d) 6; ●: case 1, □: case 2, and ▲: case 3; the horizontal axis corresponds to the x axis in Fig. 1.

tively. Figures 7 and 8(a)–8(d) show the results for $n=3$, 4, 5, and 6, respectively. The points indicated by the symbols ●, □, and ▲ are those for cases 1, 2, and 3, respectively. Table I shows the differential conductance of the metallic CNTs evaluated from the $I-V$ characteristics in each excitation scheme. The conductance depends both on the excitation cases and the structures of the CNTs.

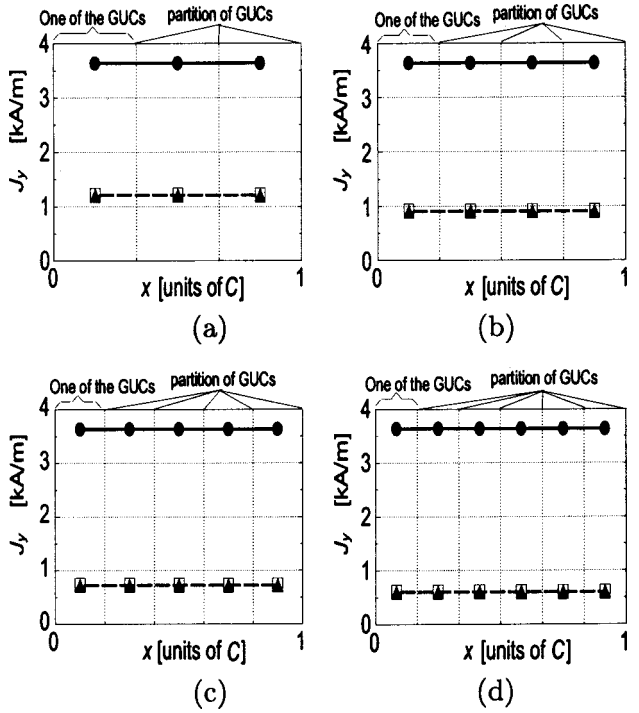

FIG. 6. Current-density distributions around the CNTs in the *armchair* CNTs: $L=20$; $n=$(a) 3, (b) 4, (c) 5, and (d) 6; ●: case 1, □: case 2, and ▲: case 3.

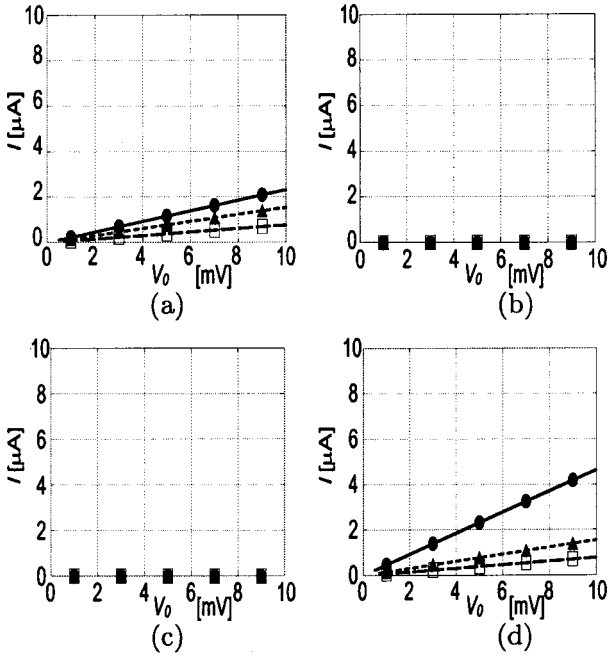

FIG. 7. $I-V$ characteristics at the *zigzag* CNTs: $L=20$; $n=$(a) 3, (b) 4, (c) 5, and (d) 6; ●: case 1, □: case 2, and ▲: case 3.

For case 1, the conductance of the CNTs with metallic *zigzag* and *armchair* structures are nG_0 and $2nG_0$, respectively, where $G_0 \equiv 2q^2/h$ is the quantum conductance. Since in every case, $f_M - f_1$ is constant under a small bias condition and the numbers of the propagation modes are always 2, the difference in the conductance can be understood by investigating the transmission coefficient $\mathcal{D}$ for each case. For case 1, the prefactor in Eq. (23) is $2q/(nh)$ and the transmission coefficients $\mathcal{D}$ become $n^2/2$ and n^2, respectively, when summed over K and K', because the current densities have sinusoidal and uniform distributions for each type. Therefore, the conductances become nG_0 and $2nG_0$, respectively.

For case 2, the conductance of the CNTs with metallic *zigzag* and *armchair* structures are G_0 and $2G_0$, respectively. This is also shown by Eq. (25). The prefactor is $2q/(nh)$ and the transmission coefficients $\mathcal{D}$ summed over K are $n/2$ and n, respectively, because the current densities also have sinusoidal and uniform distributions for each type. Therefore, the conductances are G_0 and $2G_0$, respectively.

For case 3, the conductance of the CNTs with both metallic *zigzag* and *armchair* structures is $2G_0$. This is because the prefactor is $2q/h$ and the transmission coefficient $\mathcal{D}$ is in unity in Eq. (31).

IV. POSSIBLE APPLICATION

Based on the obtained transport characteristics, we propose a ferrite device, which may work as a high-frequency filter (HFF),[9,10] as shown in Fig. 9. The operation scheme of this device is as follows: the high-frequency current flowing on one CNT may excite directly the spin waves in a ferrite film beneath it, and these are received by the other CNT. Since in this device, the operating wavelength may be con-

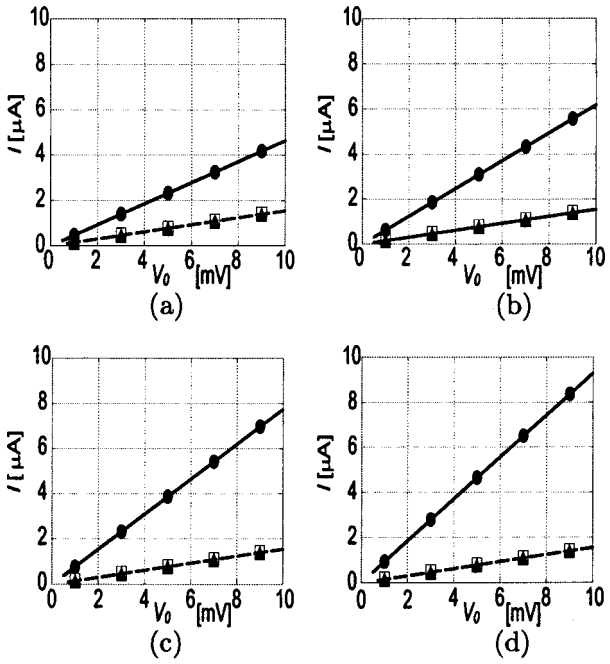

FIG. 8. $I-V$ characteristics at the *armchair* CNTs: $L=20$; $n=$(a) 3, (b) 4, (c) 5, and (d) 6; ●: case 1, □: case 2, and ▲: case 3.

trolled by means of the chirality via the current-density distributions on the CNTs, as investigated in the previous sections, this device will work as a HFF. Although this scheme is similar to that of the conventional ferrite-based microwave filters, it has been difficult in such devices to control the dimensions of the metal electrodes to within 100 nm when it is desired to extend the operating frequency up to the terahertz region. On the other hand, the diameters of the CNTs can be fabricated to scales as small as several nanometers, so that the operating frequency of the proposed device can be easily tuned to the terahertz region.

Conversely, this device may also work as a CNT chirality-discriminating device because the current distributions are significantly controlled not only by the chirality of the CNTs but also by the excitation position of the electronic waves at the input terminal.

The insertion loss (*IL*) of the device is basically defined as the ratio of the input power to the output power and is an indication of the efficiency of the device. We can improve both the *IL* and the impedance matching between the rf source and the device by increasing the CNT's conductance as much as possible, since the *IL* decreases as the conductance increases. As shown in §3, the conductance is always $2G_0$ for the intrinsic CNTs, with a metallic chirality biased at a small voltage in the excitation of case 3. In order to increase the conductance, we evaluate the characteristics of the *p*-type CNTs rather than those of the intrinsic CNTs by

TABLE I. Conductance of the metallic CNTs.

Excitation	*Zigzag*	*Armchair*
Case 1	nG_0	$2nG_0$
Case 2	G_0	$2G_0$
Case 3	$2G_0$	$2G_0$

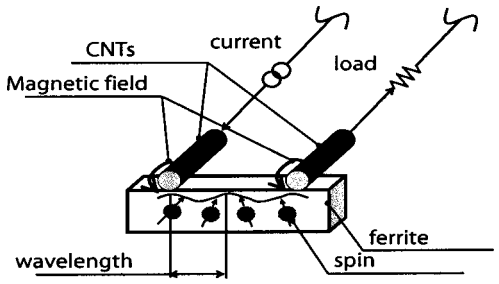

FIG. 9. The device CNTs that excite and receive directly the spin waves in a ferrite film.

changing the position of the Fermi-level E_f, that is, by changing the hole concentration in the CNTs. For the evaluation, we used the Fermi-Dirac distribution function at the left and right electrodes, respectively, as defined by Eq. (20), where, rather than using Eq. (21),

$$E^1 = \epsilon_0 + E_f \quad \text{and} \quad E^M = \epsilon_0 + E_f + V_0 \tag{32}$$

are assumed. Since it has been reported that the Fermi energy, E_f, is approximately −0.4 eV for the *p*-type CNTs,[12] we vary the E_f from 0 to −0.4 eV in our analysis.

On the other hand, the thinner the diameter of the CNTs, the higher the operating frequency of this device and the larger the *IL*. In this device, the diameters of the CNTs for $n=18$, 72, and 205 correspond to the operating wavelength of the spinwaves having frequencies of 5 THz, 1 THz, and 0.1 THz, respectively.[11] Figures 10(a)–10(d) show the $I-V$ characteristics of the *p*-type CNTs with *armchair* structures. Figures 10(a)–10(d) show the results for $n=3$, 18, 72, and 205, respectively. The points indicated by the symbols ●, □, ▲, ◇, and ▼ are those for $E_f=0$, −0.1, −0.2, −0.3, and

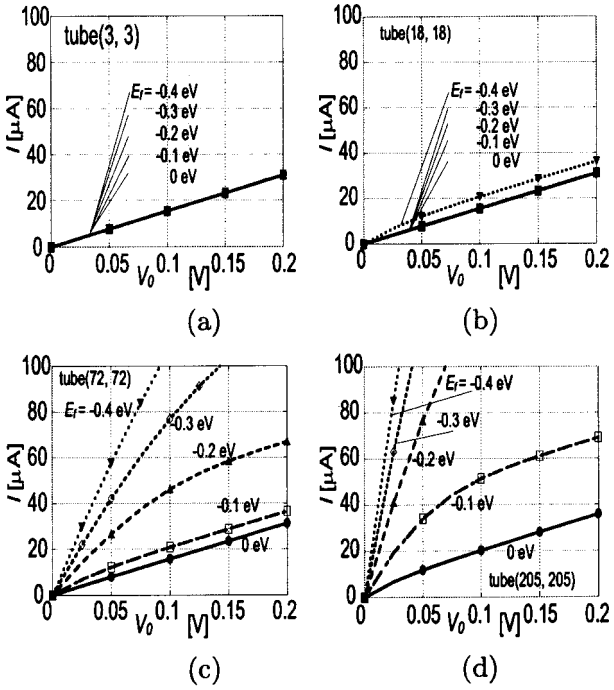

FIG. 10. $I-V$ characteristics at various Fermi levels: $L=20$; $n=$(a) 3, (b) 18, (c) 72, and (d) 205; ●: $E_f=0$ eV, □: $E_f=-0.1$ eV, ▲: $E_f=-0.2$ eV, ◇: $E_f=-0.3$ eV, and ▼: $E_f=-0.4$ eV.

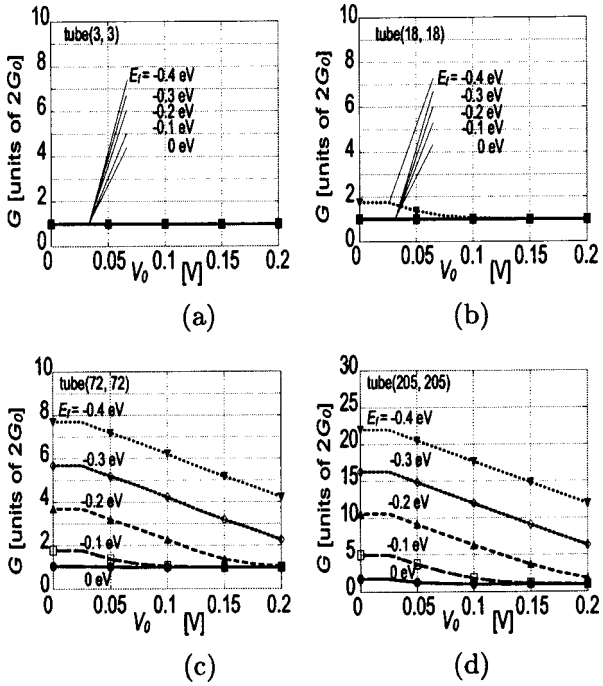

FIG. 11. $G-V$ characteristics at various Fermi levels: $G=\partial I/\partial V$, and $L=20$; $n=$(a) 3, (b) 18, (c) 72, and (d) 205; ●: $E_f=0$ eV, □: $E_f=-0.1$ eV, ▲: $E_f=-0.2$ eV, ◇: $E_f=-0.3$ eV, and ▼: $E_f=-0.4$ eV.

−0.4 eV, respectively. Figures 11(a)–11(d) show the $G-V$ characteristics for the same conditions as those of Fig. 10, where G is the differential conductance $\partial I/\partial V$.

We can improve the impedance matching between the rf source and the device by increasing the E_f, which is achieved by increasing G at a small-biased voltage. When the E_f is 0 eV, the $I-V$ characteristic is linear and G is $2G_0$. The reason is stated in the previous section. In contrast, when $|E_f|$ is larger than 0 eV, the $I-V$ characteristic is nonlinear and G is found to be larger than $2G_0$ because the numbers of the propagation modes become larger. The G for $|E_f|\neq 0$ eV increases as n becomes larger because the numbers of the propagation modes increase, as seen in Figs. 3 and 4. We can control G by means of the E_f, and E_f is controlled by changing the hole or impurity concentrations in the CNTs. From these results, we can improve the high-frequency power matching of the ferrite device by controlling G by means of E_f and n.

Although the macroscopic propagation loss of the spin wave was obtained as the value proportional to the linewidth of YIG,[13] the microscopic propagation loss should be obtained by an analysis using a model that made the CNTs and a ferrite film live together in an atomic scale. The analysis in the atomic scale is one of our future subjects.

V. CONCLUSION

We have studied the transport properties of the CNTs as coaxially rolled 2D graphite sheets based on both the LCAO and the TM methods. We have evaluated the current-density distributions around the circumference of the CNTs and the $I-V$ curves in the *zigzag* and *armchair* CNTs. The current distributions are significantly controlled by the chirality of the CNTs. More importantly, the current distributions are found to be controlled by the excitation position of the electronic waves at the input terminal. We have considered the following three specific cases of the excitation position of the electronic waves at the input terminal:

(1) the electronic waves are excited around the entire circumference of the CNT,
(2) the electronic waves are injected into the unit cell $K'=1$ of the CNT, and
(3) the electronic waves are excited uniformly around the entire circumference of the CNT and are received as an average at each unit cell of the CNT.

In cases 1 and 3, the current-density distribution around the circumference of the CNTs is uniform for any metallic chirality. In contrast, in case 2, the electric current distributions around the circumference of the CNTs are found to be nonuniform in the *zigzag* CNTs, whereas they are uniform in the *armchair* CNTs.

Based on these findings, we have proposed a ferrite device, which will work as a high-frequency bandpass filter, as well as a chirality discrimination device. The high-frequency current flowing in the CNTs may excite and receive directly the spin waves in a ferrite film, where the operating wavelength may be controlled by means of the chirality via the current-density distributions on the CNTs and the excitation position of the electronic waves at the input terminal. To improve the performance of the ferrite device, we have proposed the increasing of the conductance of the electrodes by adopting the *p*-type CNTs rather than the intrinsic CNTs. We were able to improve the matching condition by means of both the E_f and n.

In the future, we will analyze the transport characteristics of the *chiral* CNTs and the interaction between the external electromagnetic field and CNTs in order to evaluate more precisely the performance of the proposed device.

APPENDIX A: DERIVATION OF THE AVERAGE PROBABILITY CURRENT FLOW

The wave function $\Psi_{\mathbf{k}}(\mathbf{r})$ can be expressed as follows:[11]

$$\Psi_{\mathbf{k}}(\mathbf{r}) = F(\mathbf{r})\exp(\mathrm{i}\mathbf{k}\cdot\mathbf{r})u_{\mathbf{k}}(\mathbf{r}), \tag{A1}$$

where $F(\mathbf{r})$ is the amplitude and $\exp(i\mathrm{k}\cdot\mathbf{r})\mathrm{u}_{\mathbf{k}}(\mathbf{r})$ is the Bloch function. In a CNT, although $F(\mathbf{r})$ is generally a vector comprised of a set of amplitudes on each carbon atom, we treat it as a scalar for simplicity. The average probability current in the Jth CUC flowing in the y direction can be defined as follows:

$$\overline{J_J} = \int_{\mathrm{CUC}(J)} \Psi^*_{\mathbf{k}}(\mathbf{r})\frac{\hat{p}^{\mathrm{y}}}{m_0}\Psi_{\mathbf{k}}(\mathbf{r})\mathrm{d}\mathbf{r}, \tag{A2}$$

where m_0 is the electron mass. Since the amplitude $F(\mathbf{r})$ varies slowly compared to the Bloch functions, we can obtain the following equation:

$$\frac{\hat{p}^y}{m_0}\Psi_{\mathbf{k}}(\mathbf{r}) \approx F_J\frac{\exp(i\mathbf{k}\cdot\mathbf{r})}{m_0}(\hat{p}^y + \hbar k^y)u_{\mathbf{k}}(\mathbf{r}),$$

(in the Jth CUC). (A3)

From this equation, the average probability current flow can be expressed as follows:

Applying operator $\hat{p}^y$ to Eq. (A3), we have the following equation:

$$\hat{p}^{y2}\Psi_{\mathbf{k}}(\mathbf{r}) = F_J \exp(i\mathbf{k}\cdot\mathbf{r})(\hat{p}^y + \hbar k^y)^2 u_{\mathbf{k}}(\mathbf{r}). \quad \text{(A5)}$$

Substituting Eq. (A5) into the Schrödinger equation, we obtain

$$H(\mathbf{k})u_{\mathbf{k}}(\mathbf{r}) = Eu_{\mathbf{k}}(\mathbf{r}), \quad \text{(A6a)}$$

$$H(\mathbf{k}) = \frac{(\hat{p}^y + \hbar k^y)^2}{2m_0} + V(\mathbf{r}). \quad \text{(A6b)}$$

From Eqs. (A4) and (A6) and applying the Hellmann-Feynman theorem,[7] we finally obtain Eq. (8) as

$$\overline{J_J} = \frac{1}{\hbar}|F_J|^2 \int_{\mathrm{CUC}(J)} u^*_{\mathbf{k}}(\mathbf{r}) \frac{\partial H(\mathbf{k})}{\partial \mathrm{k}^y} u_{\mathbf{k}}(\mathbf{r}) \mathrm{d}\mathbf{r},$$

$$= |F_J|^2 \int_{\mathrm{CUC}(J)} u^*_{\mathbf{k}}(\mathbf{r}) \frac{1}{\hbar} \frac{\partial E(\mathbf{k})}{\partial \mathrm{k}^y} u_{\mathbf{k}}(\mathbf{r}) \mathrm{d}\mathbf{r},$$

$$= \frac{1}{\hbar} \frac{\partial E(\mathbf{k})}{\partial k^y} |F_J|^2. \quad \text{(A7)}$$

APPENDIX B: APPLYING THE BOUNDARY CONDITIONS TO THE *X* DIRECTION

The probability current flow toward the x direction $\overline{J^x_{J,K}}$ is expressed as

$$\overline{J^x_{J,K}} = \frac{1}{\hbar} \frac{\partial E}{\partial k^x_{J,K}} |F_{J,K}|^2. \quad \text{(B1)}$$

To conserve the average probability current flow and the probability density, we can impose boundary conditions, such that the current is flowing toward the y direction as

$$\begin{cases} F_{J,K} & \text{is continuous at the interface,} \\ \dfrac{1}{\hbar}\dfrac{\partial E}{\partial k^x_{J,K}} F_{J,K} & \text{is continuous at the interface.} \end{cases} \quad \text{(B2)}$$

The amplitude in the Kth GUC is expressed as

$$F_{J,K}(x,y) = \{A_{J,K}\exp[ik^x(x - x^C_{J,K})] + C_{J,K} \times \exp[-ik^x(x - x^C_{J,K})]\}\exp[ik^y_J(y - y^C_{J,K})] + \{B_{J,K}\exp[ik^x(x - x^C_{J,K})] + D_{J,K} \times \exp[-ik^x(x - x^C_{J,K})]\}\exp[-ik^y_J(y - y^C_{J,K})], \quad \text{(B3)}$$

where the coordinates x and y run within the GUC and we let $k^x \equiv k^x_{J,K}$, because it is independent of J and K. The amplitude $F_{J,K}(x,y)$ can be expressed in terms of the propagating waves toward the circumferential directions of clockwise (+) and counterclockwise (−) as

$$F^{x+}_{J,K}(x,y) = \{A_{J,K}\exp[ik^y_{J,K}(y - y^C_J)] + B_{J,K} \times \exp[-ik^y_{J,K}(y - y^C_J)]\}\exp[ik^x(x - x^C_K)], \quad \text{(B4a)}$$

$$F^{x-}_{J,K}(x,y) = \{C_{J,K}\exp[ik^y_{J,K}(y - y^C_J)] + D_{J,K} \times \exp[-ik^y_{J,K}(y - y^C_J)]\}\exp[-ik^x(x - x^C_K)]. \quad \text{(B4b)}$$

Applying the continuity conditions in Eq. (B2), we obtain the following conditions at the interface $x = (x^C_K + x^C_{K+1})/2$, $(y^C_{J-1} + y^C_J)/2 < y \leqslant (y^C_J + y^C_{J+1})/2$:

$$F^{x+}_{J,K} + F^{x-}_{J,K} = F^{x+}_{J,K+1} + F^{x-}_{J,K+1}, \quad \text{(B5a)}$$

$$\frac{\partial E}{\partial k^x_{J,K}} F^{x+}_{J,K} - \frac{\partial E}{\partial k^x_{J,K}} F^{x-}_{J,K} = \frac{\partial E}{\partial k^x_{J,K}} F^{x+}_{J,K+1} - \frac{\partial E}{\partial k^x_{J,K}} F^{x-}_{J,K+1}. \quad \text{(B5b)}$$

Equations (B5a) and (B5b) are expressed as

$$A_{J,K+1} + B_{J,K+1} = R(A_{J,K} + B_{J,K}), \quad \text{(B6a)}$$

$$C_{J,K+1} + D_{J,K+1} = \frac{1}{R}(C_{J,K} + D_{J,K}), \quad \text{(B6b)}$$

where

$$R = \exp[ik^x(x^C_{K+1} - x^C_K)] = \exp(ik^x x_G), \quad \text{(B7a)}$$

$$x_G = x^C_{K+1} - x^C_K. \quad \text{(B7b)}$$

Because there is no reflection at the output terminal $J = 1$, we have

$$B_{1,K} = D_{1,K} = 0,\ K = 1,2,\ldots,N. \quad \text{(B8)}$$

Because the propagating waves toward the circumferential directions of clockwise (+) and counterclockwise (−) have the reciprocity, the absolute values of the amplitudes $A_{1,K}$ and $C_{1,K}$ are equal and $A_{1,K}$ and $C_{1,K}$ can be equal at $K = K'$ as

$$A_{1,K'} = C_{1,K'}. \quad \text{(B9)}$$

From Eqs. (B6)–(B9), we obtain the following relation for the amplitudes as:

$$A_{1,K} + C_{1,K} = 2\cos[(K - K')k^x x_G]A_{1,1}. \quad \text{(B10)}$$

APPENDIX C: CALCULATION OF THE CURRENT DENSITY

The current density $\mathcal{J}_K$ is expressed as

$$\mathcal{J}_K = \int_{r_{CNT}}^{r_{CNT}+\delta z} n_c q v^y dz, \quad \text{(C1)}$$

where,

$$n_c = \frac{1}{(2\pi)^3}\int d^3k \times 2\{f_M(E)[1 - f_1(E)] - f_1(E)[1 - f_M(E)]\}\mathcal{D}_K, \quad \text{(C2a)}$$

$$v^y = \frac{1}{\hbar}\frac{\partial E}{\partial k^y} = \frac{1}{\hbar}\frac{dE}{dk^y}. \tag{C2b}$$

Equation (C1), where $d^3k = dk^x dk^y dk^z$, $0 < k^x \leqslant 2\pi/a$, $0 < k^y \leqslant 4\pi/\sqrt{3}a$, and $0 < k^z \leqslant 2\pi/\delta z$ for the *zigzag* types, is expressed as

$$\mathcal{J}_K = \int_{r_{CNT}}^{r_{CNT}+\delta z} dz \frac{1}{(2\pi)^3} \int_0^{2\pi/a} dk^x \int_0^{4\pi/\sqrt{3}a} dk^y \int_0^{2\pi/\delta z} dk^z$$

$$2\{f_M(E) - f_1(E)\}\frac{q}{\hbar}\frac{dE}{dk^y}\mathcal{D}_K. \tag{C3}$$

In Eq. (C3),

$$\int_{r_{CNT}}^{r_{CNT}+\delta z} dz = [z]_{r_{CNT}}^{r_{CNT}+\delta z} = \delta z, \tag{C4}$$

using $k^x = 2\pi i^x / N x_G$,

$$\int_0^{2\pi/a} dk^x = \frac{2\pi}{N x_G}\int di^x = \frac{2\pi}{N x_G}\sum_{i^x}^{1st-BZ}, \tag{C5}$$

$$\int_0^{4\pi/\sqrt{3}a} dk^y \frac{dE}{dk^y} = \int_{-\infty}^{\infty} dE, \tag{C6}$$

$$\int_0^{2\pi/\delta z} dk^z = [k^z]_0^{2\pi/\delta z} = \frac{2\pi}{\delta z}. \tag{C7}$$

From Eqs. (C4)–(C7), we obtain the following current density as:

$$\mathcal{J}_K = \frac{q}{\pi\hbar}\frac{1}{N x_G}\sum_{i^x}^{1st-BZ}\int_{-\infty}^{\infty} dE\{f_M(E) - f_1(E)\}\mathcal{D}_K. \tag{C8}$$

[1] S. Iijima, Nature (London) **354**, 56 (1991).
[2] P. R. Wallace, Phys. Rev. **71**, 622 (1947).
[3] K. Okahara, K. Tanaka, H. Aoki, T. Sato, and T. Yamabe, Chem. Phys. Lett. **219**, 462 (1994).
[4] R. Tsu and L. Esaki, Appl. Phys. Lett. **22**, 562 (1973); H. Mizuta and T. Tanoue, *The Physics and Applications of Resonant Tunneling Diodes* (Cambridge University Press, Cambridge, 1995).
[5] Y. Ando and T. Ito, J. Appl. Phys. **61**, 1497 (1987).
[6] H. Hellmann, *Einhurung in die Quanten Theorie*, (Deuticke, Leipzig, Germany, (1937); R. P. Feynman, Phys. Rev. **56**, 340 (1939).
[7] C. Yi-P. Chao and S. L. Chuang, Phys. Rev. B **43**, 7027 (1991).
[8] T. Ando, S. Wakahara, and H. Akera, Phys. Rev. B **40**, 11609 (1989).
[9] T. Umegaki, M. Ogawa, Y. Makino, and T. Miyoshi, *Quantum Transport in Carbon Nanotubes with Arbitrary Chirality*, Proceedings of the 22nd Japan Simulation Conference, Kobe, Japan, 18–19 June 2003 (Kobe University, Japan, 2004) Vol. 5–9, pp. 137–140.
[10] T. Umegaki, M. Ogawa, and T. Miyoshi, "An Analysis of Spin Waves Excited in Ferrites by Carbon Nanotubes," Extended Abstracts of the 51st Autumn Meeting, 31a-E-4 (2003), The Japan Society of Applied Physics and Related Societies (Kobe University, Japan, 2004).
[11] C. Hamaguchi, *Basic Semiconductor Physics* (Springer-Verlag, Berlin, 2001).
[12] J. G. Wildöer, L. C. Venema, A. G. Rinzler, R. E. Smalley, and C. Dekker, Nature (London) **391**, 59 (1998).
[13] S. N. Bajpai, R. L. Carter, and J. M. Owens, IEEE Trans. Microwave Theory Tech. **36**, 132 (1988).